Oligomerization and Polymerization Steps in Remote Plasma Chemical Vapor Deposition of Silicon–Carbon and Silica Films from Organosilicon Sources

A. M. Wróbel* and A. Walkiewicz-Pietrzykowska

*Centre of Molecular and Macromolecular Studies, Polish Academy of Sciences,
Sienkiewicza 112, PL-90-363 Łódź, Poland*

Y. Hatanaka, S. Wickramanayaka,[†] and Y. Nakanishi

Research Institute of Electronics, Shizuoka University, Hamamatsu 432, Japan

Received March 20, 2000

Remote hydrogen and remote oxygen plasma chemical vapor depositions (RHP–CVD and ROP–CVD, respectively) of amorphous hydrogenated silicon–carbon (a-Si:C:H) and amorphous silica (a-SiO₂) films, respectively, from organosilicon source compounds were selected as model processes for the mechanistic study. Hexamethyldisilane (HMDS) and trimethylsilane (TrMS) source compounds were used for RHP–CVD, whereas tetraethoxysilane (TEOS) was a source compound for ROP–CVD. The reactivity of HMDS and TrMS with atomic hydrogen and TEOS with atomic oxygen was characterized by determining the rate constants of RHP–CVD and ROP–CVD, respectively. On the basis of the values of the rate constants, the identified low-molecular-weight and oligomeric products collected from the gas phase, and the chemistry involved in their formation, the mechanisms of the precursors formation step are proposed. The results provide strong evidence for the gas-phase conversion of HMDS and TrMS to 1,1-dimethylsilene, Me₂Si=CH₂, and TEOS to diethoxysilanone, (EtO)₂Si=O, transient intermediates as major precursors to the a-Si:C:H and a-SiO₂ films, respectively. Owing to the high-reactivity π-bonds in the silene (>Si=C<) and silanone (>Si=O) units, the precursors may readily undergo polymerization. A hypothetical mechanism of the polymerization and cross-linking steps contributing to the growth of the a-Si:C:H and a-SiO₂ films are discussed.

1. Introduction

Remote plasma chemical vapor deposition (CVD), also termed indirect or downstream plasma CVD, has become in recent years an important method for the fabrication of defect-free, high-quality thin-film materials for advanced technology.[1,2] This technique substantially differs from conventional, direct plasma CVD in two major aspects. The first is that the plasma generation and film deposition takes place in spatially separated regions. Second is that the plasma is induced in a region free of a source compound, unlike direct plasma CVD, using a simple, non-film-forming gas that is either chemically inert (e.g., argon and helium) or reactive (e.g., hydrogen, oxygen, nitrogen, and ammonia).[1,2] The selected active and electrically neutral species are fed from the plasma region, through the remote section (trap for electrons, ions, and ultraviolet photons) to the deposition zone where they initiate the CVD process.

Owing to these aspects, the remote plasma CVD offers well-controlled growth conditions, free of film-damaging effects, such as charged-particle bombardment or high-energy ultraviolet irradiation that often occur in the direct plasma CVD.[3]

In the present study we use a molecular hydrogen and molecular oxygen as the upstream gases for plasma generation. In this case, the CVD process can be initiated in a homogeneous step, with an exclusive contribution of atomic hydrogen[4–6] or atomic oxygen.[7–9] This enables one to predict the chemistry of the CVD process, which is determined by the reactivity of the source compound with the hydrogen or oxygen radicals. The recent studies showed that RHP–CVD was successfully used for the fabrication of a broad class of thin-

* To whom correspondence should be addressed. E-mail: amwrobel@bilbo.cbmm.lodz.pl.
† Present address: ANELVA Corporation, R&D Division, Tokyo 183, Japan.

(1) Lucovsky, G.; Tsu, D. V.; Rudder, R. A.; Markunas, R. J. In *Thin Film Processes II*; Vossen, J. L., Kern, W., Eds.; Academic: Boston, MA, 1991; Chapter 4.
(2) Luft, W.; Tsuo, W. Y. *Hydrogenated Amorphous Silicon Alloy Deposition Process*; Marcel Dekker: New York, 1993; Chapter 9.

(3) Wróbel, A. M.; Czeremuszkin, G. *Thin Solid Films* **1992**, *216*, 203.
(4) Wróbel, A. M.; Wickramanayaka, S.; Hatanaka, Y. *J. Appl. Phys.* **1994**, *76*, 558.
(5) Wróbel, A. M.; Wickramanayaka, S.; Nakanishi, Y.; Hatanaka, Y.; Wysiecki, M. *J. Chem. Vap. Deposition* **1994**, *2*, 229.
(6) Wróbel, A. M.; Walkiewicz-Pietrzykowska, A.; Stasiak, M.; Aoki, T.; Hatanaka, Y.; Szumilewicz, J. *J. Electrochem. Soc.* **1998**, *145*, 1060.
(7) Wickramanayaka, S.; Meikle, S.; Sekiguchi, A.; Hosokawa, N.; Hatanaka, Y. *J. Appl. Phys.* **1991**, *69*, 6340.
(8) Wickramanayaka, S.; Meikle, S.; Kobayashi, T.; Hosokawa, N.; Hatanaka, Y. *J. Vac. Sci. Technol. A* **1991**, *9*, 2999.
(9) Wickramanayaka, S.; Hosokawa, N.; Hatanaka, Y. *Jpn. J. Appl. Phys.* **1991**, *30*, 2897.

film materials comprising silicon-based films: amorphous hydrogenated silicon (a-Si:H),[10−15] silicon carbide (a-Si:C:H),[5,16−21] silicon nitride (a-Si:N:H),[22−24] and metal-based films (Zn:S:Se,[25] Ga:As,[26] copper[27]) whereas ROP−CVD was used for the production of a high-quality amorphous silica (a-SiO$_2$) films.[28−31] Although the structure and properties of the films produced by the remote plasma CVDs were studied extensively, knowledge of the chemistry involved in these processes is poor as yet. Therefore, we have undertaken a mechanistic study related to the formation of two technologically important thin-film materials, namely, a-Si:C:H and a-SiO$_2$, which in the present work are produced from hexamethyldisilane (HMDS) and trimethylsilane (TrMS) by RHP−CVD and from tetraethoxysilane (TEOS) by ROP−CVD, respectively. In contrast to hazardous mixtures of silane (SiH$_4$) with a hydrocarbon (CH$_4$, C$_2$H$_4$, and C$_2$H$_2$) or with an oxidizer (O$_2$, O$_3$, and N$_2$O), which are often applied for the fabrication of the a-Si:C:H or a-SiO$_2$ films, respectively, the use of organosilicon source compounds is particularly beneficial for the following reasons: they are carriers of the S−C or Si−O bonds, which are readily incorporated into the deposit; they are easy to convert to film-forming precursors; and they are nonexplosive, nonflammable, nontoxic, and inexpensive. Regarding TEOS, it is worthwhile mentioning that production of silica films from this source compound constitutes one of the most prominent achievements of the CVD technique, which has gained wide interest in VLSI (very-large-scale integration) technology.[32−34]
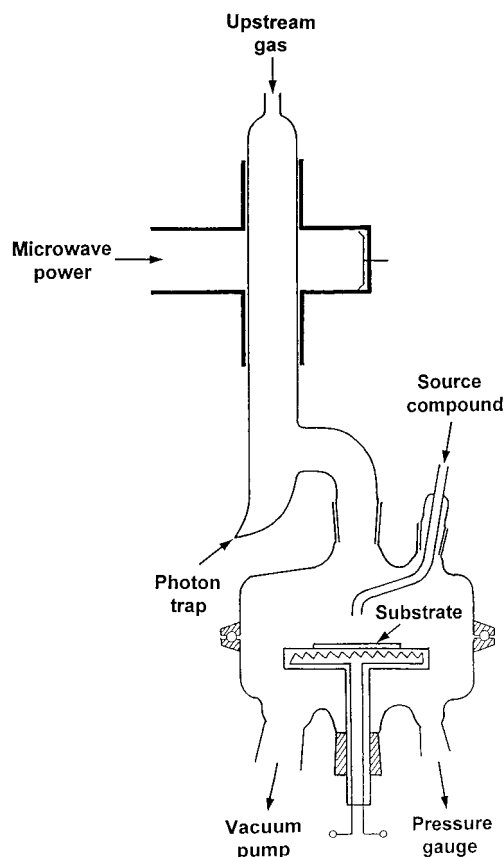

Figure 1. Scheme of the remote plasma CVD apparatus used for film deposition.

To get insight into the mechanism of the reactions contributing to the investigated RHP−CVD and ROP−CVD processes and into the chemical nature of film-forming precursors, we have performed the examination of the low-molecular-weight gas-phase conversion products of the source compounds by means of high-resolution gas chromatography/mass spectrometry (GC/MS). This combined technique appeared to be very powerful for indirect diagnosis of the gas phase in direct plasma CVD.[35−37] On the basis of the identified gas-phase intermediates, kinetics of film growth, and structure of the films, the mechanisms of the precursors formation step are proposed. Hypothetical mechanisms of subsequent oligomerization and polymerization of the precursors are discussed in terms of their contribution to growth of the a-Si:C:H and a-SiO$_2$ films.

2. Experimental Section

2.1. Remote Plasma CVD Systems. The remote plasma CVD system used for the production of a-Si:C:H is schematically shown in Figure 1. The apparatus consists of three major parts: a plasma generation section (made of a Pyrex glass tube, 28-mm i.d.) coupled via a resonant cavity and a waveguide with a 2.45 GHz microwave power supply unit; a remote section equipped with a Wood's horn photon trap; a CVD reactor (made of Pyrex glass by HWS, Mainz) containing

(10) Yoshida, A.; Inoue, K.; Ohashi, H.; Saito, Y. *Appl. Phys. Lett.* **1990**, *57*, 484.
(11) Meikle, S.; Nakanishi, Y.; Hatanaka, Y. *Jpn. J. Appl. Phys.* **1990**, *29*, L2130.
(12) Meikle, S.; Nakanishi, Y.; Hatanaka, Y. *J. Vac. Sci. Technol. A* **1991**, *9*, 1051.
(13) Johnson, N. M.; Nebel, C. E.; Santos, P. V.; Jackson, W. B.; Street, R. A.; Stevens, K. S.; Walker, J. *Appl. Phys. Lett.* **1991**, *59*, 1443.
(14) Kawasaki, M.; Suzuki, H. *J. Appl. Phys.* **1994**, *75*, 3456.
(15) Kim, D.-H.; Park, Y.-B.; Lee, I.-J.; Rhee, S.-W. *J. Electrochem. Soc.* **1996**, *143*, 2640.
(16) Yasui, K.; Fujita, A.; Akahane, T. *Jpn. J. Appl. Phys.* **1992**, *31*, L379.
(17) Yasui, K.; Muramoto, M.; Akahane, T. *Jpn. J. Appl. Phys.* **1994**, *33*, 4395.
(18) Wickramanayaka, S.; Hatanaka, Y. Nakanishi, Y.; Wróbel, A. M. *J. Electrochem. Soc.* **1994**, *141*, 2910.
(19) Wróbel, A. M.; Wickramanayaka, S.; Nakanishi, Y.; Fukuda, Y.; Hatanaka, Y. *Chem. Mater.* **1995**, *7*, 1403.
(20) Wróbel, A. M.; Wickramanayaka, S.; Nakanishi, Y.; Hatanaka, Y. *J. Mater. Process. Technol.* **1995**, *53*, 477.
(21) Wróbel, A. M.; Wickramanayaka, S.; Nakanishi, Y.; Hatanaka, Y.; Pawlowski, S.; Olejniczak, W. *Diamond Relat. Mater.* **1997**, *6*, 1081.
(22) Yasui, K.; Nasu, M.; Komaki, K.; Kaneda, S. *Jpn. J. Appl. Phys.* **1990**, *29*, 918.
(23) Yasui, K.; Nasu, M.; Kaneda, S. *Jpn. J. Appl. Phys.* **1990**, *29*, 2822.
(24) Aoki, T.; Ogishima, T.; Wróbel, A. M.; Nakanishi, Y.; Hatanaka, Y. *Vacuum* **1998**, *51*, 747.
(25) Fujiwara, H.; Gotoh, J.; Shirai, H.; Shimizu, I. *J. Appl. Phys.* **1993**, *74*, 5510.
(26) Sato, M. *Jpn. J. Appl. Phys.* **1995**, *34*, L93.
(27) Aoki, T.; Wickramanayaka, S.; Wróbel, A. M.; Nakanishi, Y.; Hatanaka, Y. *J. Electrochem. Soc.* **1995**, *142*, 166.
(28) Selamoglu, N.; Mucha, J. A.; Ibbotson, D. E.; Flamm, D. L. *J. Vac. Sci. Technol. B* **1989**, *7*, 1345.
(29) Chang, C. P.; Pai, C. S.; Hsieh, J. J. *J. Appl. Phys.* **1990**, *67*, 2119.
(30) Pai C. S.; Chang, C. P. *J. Appl. Phys.* **1990**, *68*, 793.
(31) Wickramanayaka, S.; Matsumoto, A.; Nakanishi, Y.; Hosokawa, N.; Hatanaka, Y. *Jpn. J. Appl. Phys.* **1994**, *137*, 2209.
(32) Adams, A. C. In *VLSI Technology*; Sze, S. M., Ed.; McGraw-Hill: New York, 1988; Chapter 6, pp 235−260.
(33) Barron, A. R. *Adv. Mater. Opt. Electron.* **1996**, *6*, 101.
(34) Ray, S. K.; Maiti, C. K.; Lahiri, S. K.; Chakrabarti, N. M. *Adv. Mater. Opt. Electron.* **1996**, *6*, 73.
(35) Wróbel, A. M.; Czeremuszkin, G.; Szymanowski, H.; Kowalski, J. *Plasma Chem. Plasma Process.* **1990**, *11*, 277.
(36) Wróbel, A. M.; Stańczyk, W. *Chem. Mater.* **1994**, *6*, 1766.
(37) Wróbel, A. M.; Walkiewicz-Pietrzykowska, A. *J. Chem. Vap. Deposition* **1995**, *4*, 87.
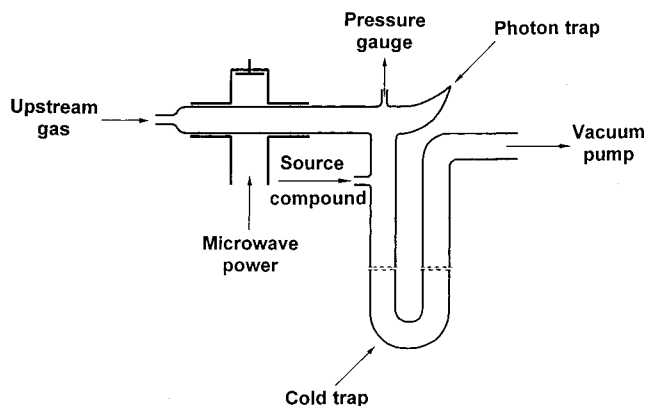
Figure 2. Scheme of the remote plasma CVD system used for collecting the low-molecular-weight products of the source compound conversion.

greaseless conical joints, 20-cm-diameter flat flanges sealed with an O-ring, and stainless steel 13-cm-diameter substrate holder equipped with a heater. A source compound injector (4-mm i.d.) is located approximately 4 cm in front of the substrate holder. Deposition experiments were performed at total pressure $p = 0.56$ Torr (75 Pa), hydrogen flow rate $F(H_2) = 100$ sccm, and microwave power input $P = 150$ W. HMDS and TrMS source compounds were fed into the CVD reactor at the evaporation temperatures of 20–25 °C; tetramethylsilane (TMS) used as a model compound was evaporated at 0 °C. The flow rate of the source compounds was $F = 0.8–5.4 \times 10^{-3}$ g min^{-1} = 0.1–0.8 sccm for HMDS, $F = 0.7–2.8 \times 10^{-3}$ g min^{-1} = 0.2–0.8 sccm for TrMS, and $F = 2.6 \times 10^{-3}$ g min^{-1} = 0.7 sccm for TMS. The flow rate of hydrogen was controlled using a MKS mass flow controller. In the case of the source compounds, a mass flow controller was used to maintain a constant flow and the flow rate was estimated gravimetrically.

Silica films were deposited in a remote plasma CVD apparatus (made of Pyrex glass) essentially similar to that shown in Figure 1 and described in detail previously.[4,5,19] In this case, oxygen plasma was generated inductively with a coil coupled via a matching network with a 13.56-MHz radio frequency power supply unit. Films were deposited under the following conditions: total pressure $p = 1$ Torr (133.3 Pa), oxygen flow rate $F(O_2) = 30$ sccm, radio frequency power input $P = 0.1–0.8$ kW, and substrate (or deposition) temperature $T_S = 300$ °C. TEOS was injected at a flow rate $F = 0.5$ sccm by evaporation at 25 °C. For the observation of chemiluminescence in the reaction zone a quartz window was applied in the CVD reactor.

In both remote plasma CVD systems the distance between the plasma edge and the substrate was 40 cm. No film deposition was observed in the plasma section, indicating that there was no back diffusion of the source compounds. Films were deposited on Fisher microscope cover glass plates (45 × 50 × 0.2 mm) and on p-type c-Si wafers.

The remote plasma CVD system used for the production and collection of low-molecular-weight gas-phase products is schematically illustrated in Figure 2. The apparatus made of Pyrex glass tube (3-cm i.d.) is composed of a plasma generation section, with a microwave resonant cavity, coupled via a waveguide with a microwave (2.45 GHz) power source, and a remote section (bent tube) equipped with a photon trap, and containing the source compound vapor inlet (4-mm i.d.): U-shaped cold trap immersed in a liquid nitrogen, in the case of RHP–CVD, or in a cooling mixture of acetone with dry ice, in the case of ROP–CVD. The distance between the plasma edge and the source compound inlet is about 40 cm. The length of the reaction tube is 20 cm. The low-molecular-weight products were produced for 2 h at power inputs of 150 and 120 W for RHP–CVD and ROP–CVD, respectively, and at the same operating parameters as specified above for the deposition experiments.

2.2. Titration of the H and O Atoms. The concentration of atomic hydrogen in the CVD reactor was estimated by the titration with nitric dioxide using a titration method and an apparatus described earlier.[6,8,9] The method involving injection of NO_2 gas into the downstream flow is based on monitoring the extinction of green light radiation from NO_2* chemiluminescence. The population of atomic oxygen in the reactor was determined using a titration technique and a system reported elsewhere.[7,8] According to the technique, concentration of a ground-state atomic oxygen $O(^3P)$ was estimated by the titration with nitric oxide, admitting a NO–Ar mixture into a downstream flow and monitoring the extinction of chemiluminescence emission characteristic of excited nitrogen dioxide. For determination of the concentration of excited atomic oxygen $O(^1D)$, argon in a mixture of NO–Ar was replaced by H_2, which removes $O(^1D)$. The titrations of atomic hydrogen and atomic oxygen were performed at the same operating parameters as in the deposition experiments.

2.3. GC/MS Examination. After the CVD process was finished, the products were removed from the cold trap of the remote plasma CVD system to a glass flask (not marked in Figure 2) joined to the system through a greaseless glass joint and a greaseless valve. The flask was then filled with helium to atmospheric pressure and the liquid content was sucked and injected into a Varian 3400 gas chromatograph equipped with a flame ionization detector (FID) and a 30 m × 0.25 mm capillary column DB-1. In the case of TrMS and TEOS conversion products, they were removed from the cold trap by extraction with pure tetrahydrofurane (THF). The GC column was heated from 40 to 250 °C with a linear heating rate of 10° min^{-1}. Helium carrier gas was flowing through the column with a steady rate of 0.6 cm^3 min^{-1}, in the case of HMDS products, and 1.0 cm^3 min^{-1}, in the case of TrMS and TEOS products. The separated products were analyzed with a Finnigan MAT 95 mass spectrometer coupled with a gas chromatograph. The mass spectra were recorded at the ionizing electron energy of 70 eV. Concentrations of the identified compounds, c, were evaluated from the formula $c = f \times S$, where f and S denote the response factor and the surface area of the GC peak, respectively. The approximate values of f were calculated using the formula for FID, $f = M/12 N_C$, where M is the molecular weight and N_C is the number of carbon atoms in the molecule.[38]

2.4. Spectroscopic and Related Techniques. Chemiluminescence spectra of the reaction zone during ROP–CVD were recorded by means of a Hamamatsu E990-07 photomultiplier tube in combination with a JOBIN YVON H20 UV monochromator.

Fourier transform infrared (FTIR) absorption spectra of the source compounds and the a-Si:C:H and a-SiO$_2$ films, deposited on c-Si, p-type wafers, were recorded in the transmission mode on a FTIR-Infinity ATI Matson spectrophotometer. The spectrum of gaseous TrMS source compound was taken using a gas cell, 10 cm in length, equipped with sodium chloride windows, whereas the spectrum of the HMDS liquid source compounds were recorded for about 0.1-mm-thick liquid film. Auger electron spectroscopic (AES) analysis was performed by means of an ULVAC AQM 808 system. To record the AE spectra for the bulk region (at about 100 nm in depth), the films were subjected to sputter-etching with a 2-kV Ar$^+$ beam prior to the AES analysis. Thickness of the films deposited on c-Si wafers was measured ellipsometrically using a Nippon Infrared Industrial Co. EL-101D ellipsometer equipped with a He–Ne laser.

2.5. Materials. The HMDS, TrMS, and TMS source compounds (Hüls and PCR) were of high-grade purity. TEOS (PCR) was purified by distillation over sodium. The THF solvent (Aldrich) was anhydrous and of 99.9% purity. The hydrogen and oxygen upstream gases were of 99.99% purity.

3. Results and Discussion

3.1. Atomic Hydrogen and Atomic Oxygen Sources.

In the present study, we used low-pressure

(38) Kaiser, R. *Gas Chromatography*; Butterworth: London, 1963; Vol. 1, p 117; Vol. 3, pp 99–101.
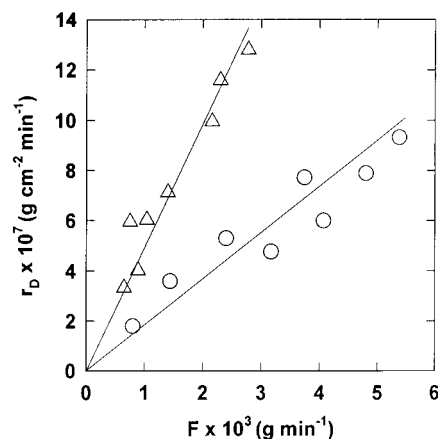
Table 1. Major Neutral Active Species Produced in the Hydrogen[39−44] and Oxygen[7,43−48] Plasmas

plasma-generating gas	neutral active species	metastable energy (eV)	radiative lifetime (s)
hydrogen	$H_2(C^3\Pi_u)$	11.75	10^{-4} to 10^{-3}
	$H(^2S)$	0	
	$H[(2p)^2P^0]$	10.20	1.6×10^{-9}
	$H[(3p)^2P^0]$	12.09	5.5×10^{-9}
oxygen	$O_2(a^1\Delta_g)$	0.98	2.7×10^3
	$O_2(b^1\Sigma_g^+)$	1.63	7.1
	$O(^3P)$	0	
	$O(^1D)$	1.97	1.5×10^2
	$O(^1S)$	4.19	0.71

plasmas of hydrogen and oxygen as the effective sources of hydrogen and oxygen atoms. As charged species and ultraviolet photons have been eliminated from the reaction zone by the remote section equipped with a photon trap (Figures 1 and 2), the neutral active species important for the investigated CVD processes have to be considered. Characteristics of the molecular and atomic active neutral species produced in the plasma of hydrogen[39−44] and oxygen[7,43−48] are shown in Table 1. The contribution of electronically excited and short radiative lifetime species, $H_2(C^3\Pi_u)$, $H[(2p)^2P^0]$, $H[(3p)^2P^0]$, $O_2(b^1\Sigma_g^+)$, and $O(^1S)$ (Table 1), to RHP−CVD and ROP−CVD, respectively, is negligible at a relatively long distance (0.4 m) between the plasma edge and the inlet of a source compound. The $O_2(a^1\Delta_g)$ species are of minor importance for ROP−CVD due to considerably small excited-state energy, which is lower than the energies of chemical bonds. Therefore, we assume that the ground-state atoms $H(^2S)$, in the case of RHP−CVD, and the ground-state $O(^3P)$ as well as electronically excited $O(^1D)$ atoms, in the case of ROP−CVD, play a major role in the initiation step.

For the RHP−CVD experiments, concentration of atomic hydrogen in the reactor was constant, $[H] = 5 \times 10^{15}$ cm^{-3}. For the ROP−CVD experiments, the total concentration of atomic oxygen $[O] = [O(^3P)] + [O(^1D)]$ and the $O(^1D)$ fraction were controlled in the reactor by the power input to the oxygen plasma and varied in the ranges $[O] = (1.5−16) \times 10^{14}$ cm^{-3} and $[O(^1D)]/[O] = 45−95\%$.

3.2. Reactivity of Source Compounds in Atomic Hydrogen and Atomic Oxygen Environments. *RHP−CVD.* The reactivity of three methylsilane compounds, HMDS, TrMS, and TMS, in the investigated RHP−CVD have been examined in a qualitative way, that is, by their ability to form film. Inability of film formation found for TMS indicates that the C−H and Si−C bonds are nonreactive in the initiation step. It is

(39) Bell, A. T. *Ind. Eng. Chem. Fundam.* **1972**, *11*, 209.
(40) Baravian, G.; Chouan, Y.; Ricard, A.; Sultan, G. *J. Appl. Phys.* **1987**, *61*, 5249.
(41) Kushner, M. J. *J. Appl. Phys.* **1988**, *63*, 2532.
(42) Rousseau, A.; Granier, A.; Gousset, G.; Leprince, P. *J. Phys. D: Appl. Phys.* **1994**, *27*, 1412.
(43) Vossen J. L.; Cuomo, J. J. In *Thin Film Processes*; Vossen, J. L., Kern, W., Eds.; Academic: New York, 1978; Chapter 2.1, p 46.
(44) Okabe, H. *Photochemistry of Small Molecules*; Wiley-Interscience: New York, 1978.
(45) Bell, A. T.; Kwong, K. *Ind. Eng. Chem. Fundam.* **1973**, *12*, 90.
(46) Hadj-Ziane, S.; Held, B.; Pignolet, P.; Coste, C. *J. Phys. D: Appl. Phys.* **1992**, *28*, 677.
(47) Kushner, M. J. *J. Appl. Phys.* **1993**, *74*, 6538.
(48) Lee, C.; Graves, D. B.; Lieberman, M. A.; Hess, D. W. *J. Electrochem. Soc.* **1994**, *141*, 1546.

Figure 3. Deposition rate r_D of a-Si:C:H film as a function of the source compound flow rate F determined for HMDS (○) and TrMS (△).

noteworthy that TMS easily forms film in the direct plasma CVD.[35−37] Capability of HMDS and TrMS for film formation, resulting from the deposition experiments, accounts for susceptibility of the Si−Si and Si−H bonds, respectively, toward the reaction with atomic hydrogen.

To characterize reactivity of the HMDS and TrMS source compounds in a quantitative way, we have evaluated the yield of the RHP−CVD process (k_D) defined according to eq 1

$$k_D = r_D/F \qquad (1)$$

where r_D denotes the mass-based film deposition rate and F is the mass-based source compound flow (or feeding) rate. In a physical sense, the quantity k_D expresses mass of the deposit per unit mass of the source compound fed into the reactor and was found to be very sensitive to the molecular structure of the compound.[49,50] The quantity k_D may also be considered as the rate constant of the CVD process.[50] However, it should be noted that k_D is not strictly the rate constant of the chemical reaction. Moreover, the values of k_D calculated for the investigated CVD system cannot be directly compared with those obtained for other CVD systems. It is noteworthy that the quantity k_D has successfully been used in our earlier study for the determination of the reactivity of organosilicon[4−6,18−21,36,37] and organoisothiocyanate[51] source compounds in the RHP−CVD[4−6,18−21] and the direct plasma CVD.[36,37,51]

To evaluate k_D, we determined the deposition rate dependencies on the flow rate of the HMDS and TrMS source compounds, which are presented in Figure 3. To avoid undesirable effects, which might arise from thermally induced reactions, the RHP−CVD experiments were carried out using an unheated substrate. The quantity k_D has been calculated from the slopes of linear plots in Figure 3 and the resulting values are listed in Table 2, which for the sake of correlation, also contains the activation energy (E_a) values reported for dissocia-

(49) Gazicki, M.; Yasuda, H. *J. Appl. Polym. Sci.: Appl. Polym. Symp.* **1984**, *38*, 35.
(50) Yasuda, H. *Plasma Polymerization*; Academic: Orlando, FL, 1985; Chapter 6, pp 169−171.
(51) Wróbel, A. M.; Kryszewski, M.; Czeremuszkin, G. *Thin Solid Films* **1996**, *289*, 112.

Table 2. Correlation between the Activation Energy for Dissociation of the Si–Si and Si–H Bonds in the Gas-Phase Reactions with Atomic Hydrogen and the Rate Constant of the RHP–CVD Process for HMDS and TrMS Source Compounds

source compound	active bond	activation energy for dissociation[a] (kJ mol⁻¹)	rate constant, k_D ($\times 10^5$ cm⁻²)
hexamethyldisilane	Si–Si	27.6 or 13.4	16
trimethylsilane	Si–H	10.0	45

[a] Data for gas-phase reactions of disilane with atomic hydrogen from ref 52.

tion of the Si–Si and Si–H bonds in disilane under attack of a hydrogen atom in the gas phase.[52] Two energy barriers specified for the dissociation of the Si–Si bond correspond to the reactions involving either a frontside attack or a backside attack of a hydrogen atom on the bond (27.6 or 13.4 kJ mol⁻¹, respectively). When the rate constants presented in Table 2 are compared, a much higher value of k_D was obtained for TrMS. This evidently proves higher reactivity of the Si–H unit than that of the Si–Si unit, under the investigated conditions. Therefore, TrMS constitutes an effective source compound for the formation of the a-Si:C:H films. Moreover, the data in Table 2 reveal a reasonable correlation between E_a and k_D values, which may be expressed by the inequalities E_a(Si–H) < E_a(Si–Si) and k_D(TrMS) > k_D(HMDS). The lower activation energy for dissociation of the Si–H bond corresponds well with the higher RHP–CVD's rate constant for TrMS, as compared with respective data for HMDS.

High reactivity of the Si–H unit in RHP–CVD is demonstrated by the results of the FTIR spectroscopy presented in Figure 4a, which shows the spectra of the TrMS source compound and resulting a-Si:C:H film. The intense absorption bands corresponding to stretching and bending vibrations of Si–H units present in the spectrum of TrMS at 2110 and 910 cm⁻¹, respectively, are undetectable in the film spectrum. For comparison, Figure 4b shows the spectrum of the HMDS source compound and that of the a-Si:C:H film.

ROP–CVD. To obtain information on the reactivity of TEOS in a different environment of atomic oxygen, the ROP–CVD experiments were carried out with three power input levels: 0.1, 0.2, and 0.8 kW, at which the concentrations of atomic oxygen and its O(¹D) fractions in the CVD reactor are significantly different. To produce good-quality silica films, the experiments were performed at the substrate temperature T_S = 300 °C. The deposition rates were calculated from the slopes of the linear plots of time dependencies of film thickness determined for different power input, which are presented in Figure 5. The resulting deposition rate values are listed in Table 3. The deposition rate data from this table are plotted in Figure 6 as a function of the concentration of atomic oxygen and/or O(¹D) fraction. Two important conclusions can be inferred from a linear plot of the relationship in Figure 6: (*i*) Film deposition rate (r_D) is proportional to the concentration of atomic oxygen (eq 2) the proportionality coefficient or rate

$$r_D = k[O] \tag{2}$$

constant of ROP–CVD, calculated from the slope of the plot, is $k = 8.4 \times 10^{-22}$ cm⁴ min⁻¹. In other words, an
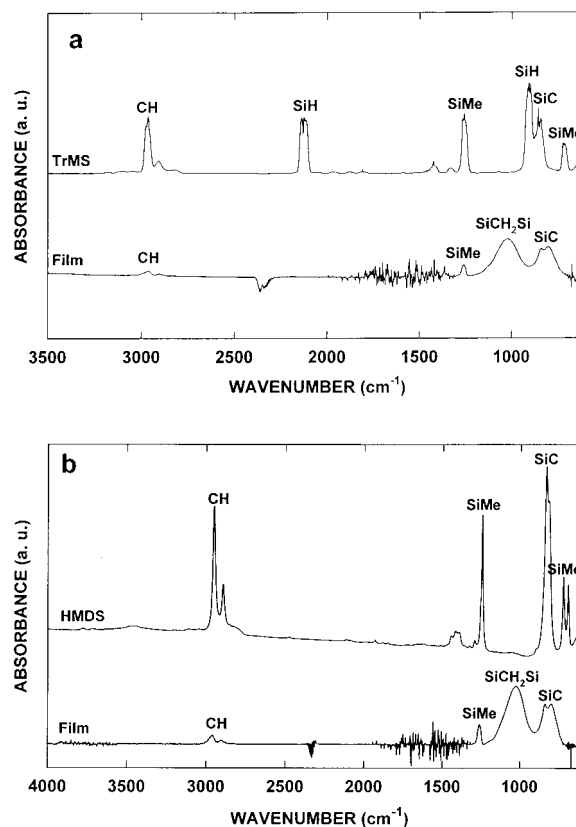

Figure 4. FTIR transmission spectra of (a) gaseous TrMS source compound and its a-Si:C:H (550-nm-thick) deposit and (b) liquid film of HMDS and its a-Si:C:H (600-nm-thick) deposit; c-Si substrate temperature, T_S = 30 °C.
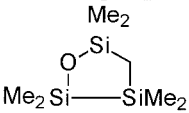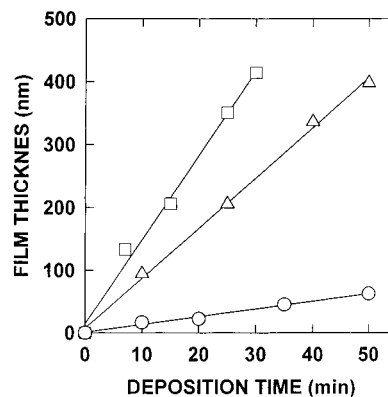

Figure 5. Deposition time dependencies of silica film thickness determined at T_S = 300 °C for various power input to oxygen plasma: 0.1 (○), 0.2 (△), and 0.8 kW (□).

Table 3. Deposition Rate of a SiO₂ Film Determined for Different Concentrations of Atomic Oxygen and O(¹D) Fraction in the Reactor Controlled by the Power Input to Oxygen Plasma

power input (kW)	atomic oxygen conc (10^{14} cm⁻³)	O(¹D) fraction (%)	deposition rate, r_D (nm min⁻¹)
0.1	1.5	45	1.2
0.2	9.7	55	8.0
0.8	16.0	95	13.4

increase in the concentration of atomic oxygen enhances TEOS conversion to silica film-forming precursors. (*ii*) Film deposition rate is not affected by the composition of the atomic oxygen population, thus suggesting that

(52) Doobs, K. D.; Doren, D. J. *J. Am. Chem. Soc.* **1993**, *115*, 3731.

Table 4. Low-Molecular-Weight Conversion Products of Hexamethyldisilane Collected during RHP–CVD and Identified by GC/MS

Compound	Molecular weight	Molecular formula	Assigned structure	Concentration (a. u.)
1	74	$Si_1C_3H_{10}$	Me_3SiH	105.5
2	162	$Si_2C_6H_{18}O_1$	$Me_3SiOSiMe_3$	8.2
3	146	$Si_2C_6H_{18}$	$Me_3SiSiMe_3$	267.3
4	146	$Si_2C_6H_{18}$	$Me_3SiCH_2SiHMe_2$	9.9
5	144	$Si_2C_6H_{16}$	$Me_2Si\langle\square\rangle SiMe_2$	1.1
6	160	$Si_2C_7H_{20}$	$Me_3SiCH_2SiMe_3$	3.7
7	160	$Si_2C_7H_{20}$	$Me_3SiCH_2CH_2SiHMe_2$	1.5
8	204	$Si_3C_7H_{20}O_1$	(cyclic structure: Me_2Si, Me_2Si, $SiMe_2$ with O and bridging CH, Me_2)	7.2
9	234	$Si_3C_9H_{26}O_1$	$Me_3SiOSiMe_2CH_2SiMe_3$	12.4
10	218	$Si_3C_9H_{26}$	$Me_3SiCH_2SiMe_2SiMe_3$	12.1
11	232	$Si_3C_{10}H_{28}$	$Me_3SiCH_2SiMe_2CH_2SiMe_3$	1.9
12	290	$Si_4C_{12}H_{34}$	$Me_3Si(Me_2SiCH_2)_2SiMe_3$	1.7
12	290	$Si_4C_{12}H_{34}$	$(Me_3SiCH_2SiMe_2)_2$	0.9
14	320	$Si_5C_{12}H_{36}$	$(Me_3Si)_2SiMeSiMe_2CH_2SiHMe_2$ or $Me_3SiSiMe_2SiMe(SiMe_3)CH_2SiHMe_2$	8.3
15	378	$Si_5C_{12}H_{36}$	$(Me_3Si)_4Si$ or $(Me_3Si)_2SiMeSiMe_2SiMe_3$	8.3
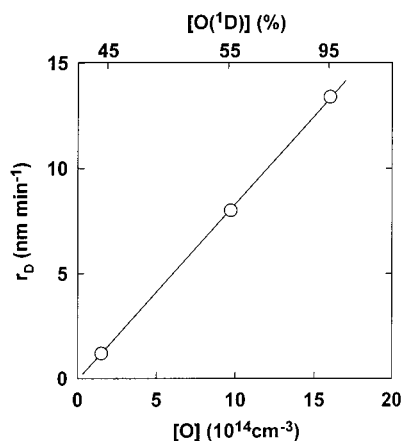
Figure 6. Deposition rate of a-SiO_2 film r_D at the substrate temperature $T_S = 300\ ^{\circ}C$ as a function of atomic oxygen total concentration [O] and/or $O(^1D)$ fraction.

both active species $O(^3P)$ and $O(^1D)$ may contribute to the precursor formation step via the same mechanism.

3.3. Gas-Phase Conversion Products of Source Compounds. *RHP–CVD.* A GC/MS examination has been performed for the conversion products of HMDS and TrMS collected from the gas phase during RHP–CVD. The gas chromatograms of the conversion products of these source compounds are shown in Figure 7a,b, respectively. The peaks in the chromatograms were identified by mass spectrometry and the summary of the identification work is presented in Tables 4 and 5, respectively, which include the individual molecular formulas, assigned molecular structures, and evaluated concentrations (in arbitrary units) of the compounds corresponding to the respective GC peaks. The differences in the retention times, which may be noted for

the same compounds identified in both gas chromatograms in Figure 7a,b arise from various flow rates of carrier gas used for performing GC/MS analyses (see Section 2.3). Moreover, a nonreacted TrMS source compound has not been recorded in the gas chromatogram in Figure 7b and therefore it is unspecified in Table 5.

The results in Tables 4 and 5 indicate that the investigated source compounds undergo conversion to a variety of low-molecular-weight and oligomeric compounds with the masses in the range of 74–320, for HMDS, and 146–320, for TrMS. The oxygen-containing compounds 2, 8, and 9 in Table 4 and compounds 8 and 11 in Table 5 are also detected. As we reported previously,[5,19] oxygen seems to be predominantly taken up during RHP–CVD and may arise from etching of the glass walls in the reaction system with atomic hydrogen.

The concentration values show that TrMS (compound 1, Table 4) and HMDS (compound 1, Table 5) appear to be the most abundant conversion products of HMDS and TrMS, respectively. Moreover, an interesting feature is the presence of linear and cyclic carbosilane products containing one or two $-Me_2SiCH_2-$ units, that is, compounds 4, 5, 6, 8, 10, 11, 12, 13, and 14 in Table 4 and compounds 2, 3, 6, and 16 in Table 5.

ROP–CVD. Figure 7c shows the high-resolution gas chromatogram of TEOS low-molecular-weight conversion products collected in the cold trap during the ROP–CVD process. Each prominent gas chromatographic peak in Figure 7c has been identified by mass spectrometry and the resulting individual molecular formulas, assigned molecular structures, and evaluated concentrations (in arbitrary units) of the compounds corresponding to the respective GC peaks are given in
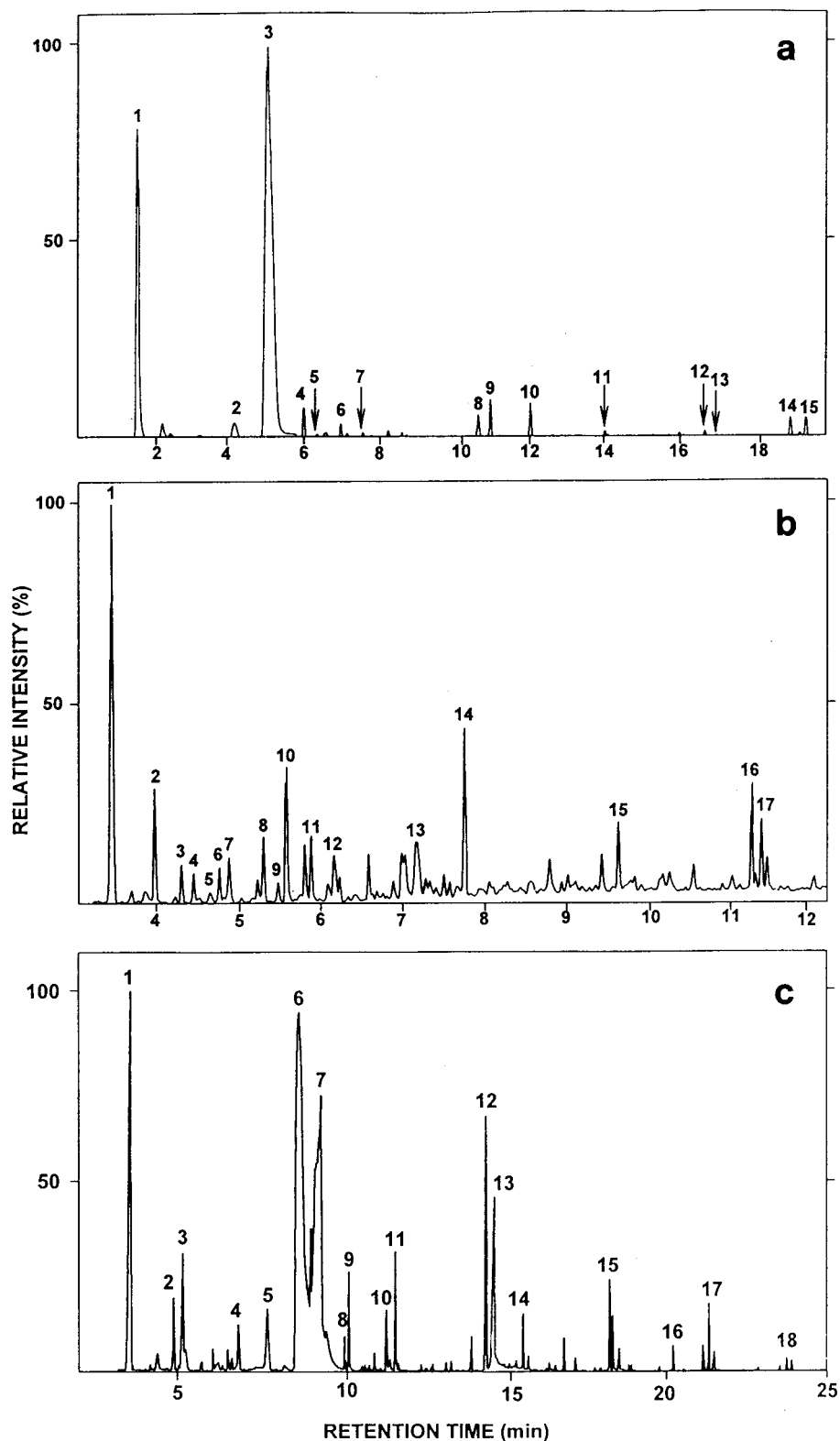
Figure 7. High-resolution gas chromatograms of low-molecular-weight conversion products of HMDS (a), TrMS (b), and TEOS (c) collected during RHP−CVD and ROP−CVD, respectively.

Table 6. It should be noted that structures of the products represented by GC peaks 6, 12, and 15 (Figure 7c) have also been verified by comparing their mass spectra with those of TEOS, hexaethoxydisiloxane, and octaethoxytrisiloxane standard compounds, respectively.

The GC/MS results shown in Table 6 indicate that TEOS undergoes conversion to a low-molecular-weight and oligomeric compounds of linear and cyclic structure with their masses ranging from 104 to 744 and containing from one to five silicon atoms. The identified structures reveal a complex chemistry of an ethoxysilyl group involved in the reactions of TEOS with atomic oxygen. The concentration data in Table 6 reveal that 2-(triethoxysilyloxy)acetaldehyde (compound 7) is the most abundant conversion product. However, much more interesting is the presence of linear oligomers 12,

Table 5. Low-Molecular-Weight Conversion Products of Trimethylsilane Collected during RHP−CVD and Identified by GC/MS
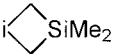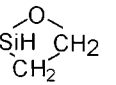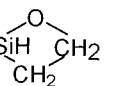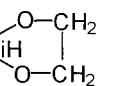
Compound	Molecular weight	Molecular formula	Assigned structure	Concentration (a. u.)
1	146	$Si_2C_6H_{18}$	$Me_3SiSiMe_3$	104.8
2	146	$Si_2C_6H_{18}$	$Me_3SiCH_2SiHMe_2$	29.7
3	144	$Si_2C_6H_{16}$	Me_2Si◇$SiMe_2$	9.7
4	162	$Si_3C_5H_{18}$	$MeH_2SiSiH_2SiMe_2Et$	10.1
5	208	$Si_5C_4H_{20}$	$Me_2HSiSiH_2SiHMeSiH_2SiH_2Me$	10.2
6	160	$Si_2C_7H_{20}$	$Me_3SiCH_2SiMe_3$	8.2
7	162	$Si_3C_5H_{18}$	$Me_3SiSiHMeSiH_2Me$	17.4
8	222	$Si_3C_7H_{22}O_2$	$Me_3SiOSiMe_2OSiHMe_2$	20.7
9	192	$Si_4C_5H_{20}$	$Me_2HSi(SiH_2)_2CH_2SiHMe_2$	9.3
10	192	$Si_4C_5H_{20}$	$Me_2HSi(SiHMe)_2SiH_2Me$	66.3
11	236	$Si_3C_8H_{24}O_2$	$Me_3SiOSiMe_2OSiMe_3$	19.4
12	206	$Si_4C_6H_{22}$	$(Me_2HSiSiHMe)_2$	23.9
13	220	$Si_4C_7H_{24}$	$Me_3SiSiHMeSiHMeSiHMe_2$	39.3
14	218	$Si_3C_9H_{26}$	$Me_3SiCH_2SiMe_2SiMe_3$	42.1
15	262	$Si_4C_{10}H_{30}$	$(Me_3SiSiMe_2)_2$	25.8
16	320	$Si_5C_{12}H_{36}$	$(Me_3Si)_3SiCH_2SiHMe_2$	32.8
17	320	$Si_5C_{12}H_{36}$	$(Me_3Si)_4Si$	31.2

Table 6. Low-Molecular-Weight Conversion Products of Tetraethoxysilane Collected during ROP−CVD and Identified by GC/MS

Compound	Molecular weight	Molecular formula	Assigned structure	Concentration (a. u.)
1	104	$Si_1C_4H_{12}O$	$EtOSiH_2Et$	83.6
2	118	$Si_1C_4H_{10}O_2$	$EtOSiH\langle O-CH_2-CH_2\rangle$	14.7
3	116	$Si_1C_4H_8O_2$	$H_2C{=}CH{-}SiH\langle O-CH_2-CH_2\rangle$	30.6
4	134	$Si_1C_5H_{14}O_2$	$(EtO)(MeO)SiHEt$	10.3
5	194	$Si_1C_7H_{18}O_4$	$(EtO)_3SiOMe$	32.5
6	208	$Si_1C_8H_{20}O_4$	$(EtO)_4Si$	208.8
7	222	$Si_1C_8H_{18}O_5$	$(EtO)_3SiOCH_2CHO$	168.4
8	222	$Si_1C_9H_{22}O_4$	$(EtO)_3SiOPr$	3.7
9	222	$Si_1C_9H_{22}O_4$	$(EtO)_3SiCH_2OEt$	14.0
9	222	$Si_2C_8H_{22}O_4$	$(EtO)_3SiOSiH_2Et$	12.3
11	268	$Si_2C_8H_{20}O_6$	$(EtO)_3SiOSiH\langle O-CH_2 \mid O-CH_2\rangle$	21.3
12	342	$Si_2C_{12}H_{30}O_7$	$(EtO)_3SiOSi(OEt)_3$	52.4
13	314	$Si_2C_{10}H_{26}O_7$	$(EtO)_3SiOSi(OH)(OEt)_2$	47.9
14	402	$Si_3C_{12}H_{30}O_9$	$[(EtO)_2SiO]_3$	6.7
15	476	$Si_3C_{16}H_{40}O_{10}$	$EtO-[(EtO)_2SiO]_2-Si(OEt)_3$	17.5
16	536	$Si_4C_{16}H_{40}O_{12}$	$[(EtO)_2SiO]_4$	4.4
17	610	$Si_4C_{20}H_{50}O_{13}$	$EtO-[(EtO)_2SiO]_3-Si(OEt)_3$	10.6
18	744	$Si_5C_{24}H_{60}O_{16}$	$EtO-[(EtO)_2SiO]_4-Si(OEt)_3$	2.3

15, 17, and 18 and cyclic oligomers 14 and 16, containing diethoxysiloxane, $-(EtO)_2SiO-$, repeating mer unit. The structure of the oligomers, which may be expressed by the general formulas $EtO-[(EtO)_2SiO]_n-Si(OEt)_3$ ($n = 1-4$) and $[(EtO)_2SiO]_n$ ($n = 3$ and 4), implies the occurrence of chain propagation, ring formation, and ring expansion reactions, respectively, with a contribution of the same precursor produced in the initiation step.
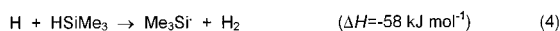
3.4. Precursor Formation Step. *RHP−CVD.* On the basis of the GC/MS results and the small amount of literature data[53−55] that report the gas-phase reac-

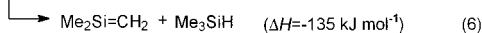(53) Jones, W. E.; Macknight, S. D.; Teng, L. *Chem. Rev.* **1973**, *73*, 407.

(54) Ellul, R.; Potzinger, P.; Reiman, B. *J. Phys. Chem.* **1984**, *88*, 2793.

(55) Fabry, L.; Potzinger, P.; Reimann, B.; Ritter, A.; Steenbergen, H. P. *Organometallics* **1986**, *5*, 1231.

tions of methylsilanes with atomic hydrogen, a mechanism for such reactions in RHP−CVD involving HMDS and TrMS can be described by eqs 3 and 4, respectively.

$$H + Me_3SiSiMe_3 \rightarrow Me_3SiH + Me_3Si^{\cdot} \quad (\Delta H = -24 \text{ kJ mol}^{-1}) \quad (3)$$

$$H + HSiMe_3 \rightarrow Me_3Si^{\cdot} + H_2 \quad (\Delta H = -58 \text{ kJ mol}^{-1}) \quad (4)$$

Trimethylsilyl radicals formed via eqs 3 and 4 may undergo either recombination or disproportionation reactions.[56,57] A secondary reaction of trimethylsilyl

$$2Me_3Si^{\blacksquare} \longrightarrow Me_3SiSiMe_3 \quad (\Delta H = -378 \text{ kJ mol}^{-1}) \quad (5)$$

$$\longrightarrow Me_2Si{=}CH_2 + Me_3SiH \quad (\Delta H = -135 \text{ kJ mol}^{-1}) \quad (6)$$

radicals with the HMDS source compound may occur.

$$Me_3Si^{\blacksquare} + Me_3SiSiMe_3 \longrightarrow Me_3SiSiMe_2\overset{\centerdot}{C}H_2 + Me_3SiH \quad (\Delta H = 37 \text{ kJ mol}^{-1}) \quad (7)$$

The radical product of eq 7 may isomerize and subsequently dissociate.[58,59] The reactions described by eqs

$$Me_3SiSiMe_2\overset{\centerdot}{C}H_2 \longrightarrow Me_3SiCH_2\overset{\centerdot}{S}iMe_2 \quad (\Delta H = -22 \text{ kJ mol}^{-1}) \quad (8)$$

$$Me_3SiCH_2\overset{\centerdot}{S}iMe_2 \longrightarrow Me_3Si^{\blacksquare} + Me_2Si{=}CH_2 \quad (\Delta H = 204 \text{ kJ mol}^{-1}) \quad (9)$$

7 and 9 are endothermic and they may, therefore, easily proceed on a heated substrate.

The presented reactions are consistent with the GC/MS data in Tables 4 and 5. Equation 3 explains well the formation of TrMS (compound 1, Table 4) as the major conversion product of HMDS, whereas eqs 4 and 5 account for the conversion of TrMS into HMDS (compound 1, Table 5) predominant product in a low-molecular-weight fraction. In accordance with our previous work 1,1-dimethylsilene $Me_2Si{=}CH_2$, a strongly reactive transient intermediate, produced via eqs 6 and 9, is considered to be an important a-Si:C:H film-forming precursor,[19] which however, is undetectable by GC/MS. The heats of the reactions involved in the precursor formation step of RHP−CVD were calculated using thermodynamic data reported by Walsh.[60]

ROP−CVD. Since the reactivity of alkoxysilanes in the atomic oxygen environment is not well understood, inferences can be made by analogy to the reactions of alkanes with oxygen atoms. Taking into account the mechanisms for the gas-phase reactions of alkanes with a ground-state $O(^3P)$[61−65] and excited-state $O(^1D)$[66−70]

(56) Tokach, S. K.; Koob, R. D. *J. Phys. Chem.* **1979**, *83*, 774.
(57) Tokach, S. K.; Koob, R. D. *J. Am. Chem. Soc.* **1980**, *102*, 376.
(58) Davidson, I. M. T.; Hughes, K. J.; Scampton, R. J. *J. Organomet. Chem.* **1984**, *272*, 11.
(59) O'Neal, H. E.; Ring, M. A. *Organometallics* **1988**, *7*, 1017.
(60) Walsh, R. In *The Chemistry of Organic Silicon Compounds*; Patai, S., Rappoport, Z., Eds.; Wiley: New York, 1989; Chapter 5, pp 371−391.
(61) Westenberg, A. A.; de Haas, N. *J. Chem. Phys.* **1967**, *46*, 490.
(62) Herron, J. T.; Huie, R. E. *J. Phys. Chem.* **1969**, *73*, 3327.
(63) Anderson, P.; Luntz, A. C. *J. Chem. Phys.* **1980**, *72*, 5842.
(64) Luntz, A. C.; Anderson, P. *J. Chem. Phys.* **1980**, *72*, 5851.
(65) Miyoshi, A.; Yamauchi, N.; Matsui, H. *J. Phys. Chem.* **1996**, *100*, 4893.
(66) Yamazaki H.; Cvetanoviæ, R. J. *J. Chem. Phys.* **1964**, *41*, 3703.
(67) Paraskevopoulos, G.; Cvetanoviæ, R. J. *J. Chem. Phys.* **1969**, *50*, 590.
(68) Paraskevopoulos, G.; Cvetanoviæ, R. J. *J. Chem. Phys.* **1970**, *52*, 5821.
(69) Michaund, P.; Cvetanoviæ, R. J. *J. Phys. Chem.* **1972**, *76*, 1375.
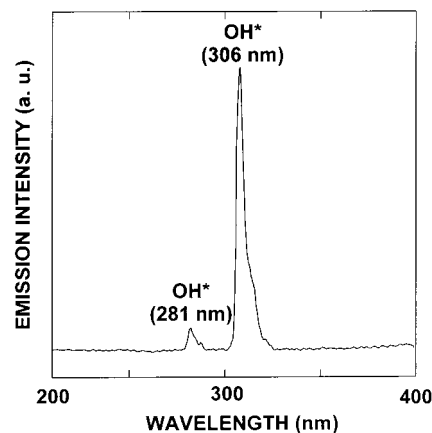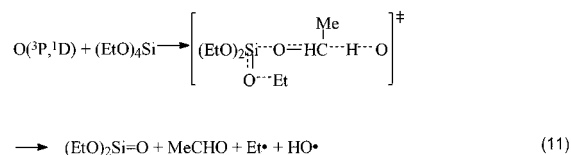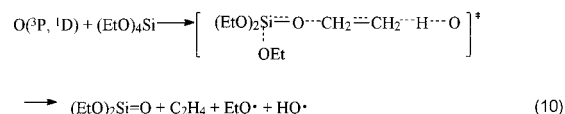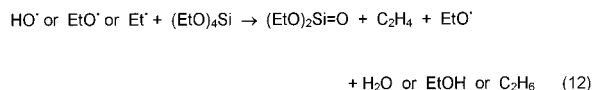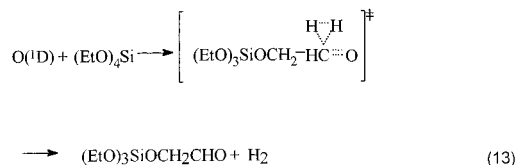(70) Luntz, A. C. *J. Chem. Phys.* **1980**, *72*, 1143.

Figure 8. Chemiluminescence spectrum of the gas phase in the CVD reactor fed with TEOS and atomic oxygen containing 55% $O(^3P)$ and 45% $O(^1D)$ fractions.

oxygen atoms and considering the structural features of TEOS, it is assumed that the abstraction of hydrogen atom from the TEOS molecule by $O(^3P)$ and $O(^1D)$ is the major step to precursor formation in the investigated ROP−CVD. The reaction may proceed via an attack by atomic oxygen on the primary or secondary hydrogen atoms in the ethoxy group as described by eqs 10 and 11, respectively. The $HO^{\bullet}$, $EtO^{\bullet}$, and $Et^{\bullet}$ radicals may

$$O(^3P, {}^1D) + (EtO)_4Si \longrightarrow \left[(EtO)_2\underset{\underset{OEt}{|}}{Si}{=\!=}O\cdots CH_2{=\!=}CH_2\cdots H\cdots O \right]^{\ddagger}$$

$$\longrightarrow (EtO)_2Si{=}O + C_2H_4 + EtO^{\bullet} + HO^{\bullet} \quad (10)$$

$$O(^3P, {}^1D) + (EtO)_4Si \longrightarrow \left[(EtO)_2\underset{\underset{O\cdots Et}{|}}{Si}{=\!=}O{=\!=}\overset{\overset{Me}{|}}{H}C\cdots H\cdots O \right]^{\ddagger}$$

$$\longrightarrow (EtO)_2Si{=}O + MeCHO + Et^{\bullet} + HO^{\bullet} \quad (11)$$

subsequently undergo secondary reactions with TEOS as exemplified by eq 12. Diethoxysilanone resulting from

$$HO^{\cdot} \text{ or } EtO^{\cdot} \text{ or } Et^{\cdot} + (EtO)_4Si \rightarrow (EtO)_2Si{=}O + C_2H_4 + EtO^{\cdot}$$

$$+ H_2O \text{ or } EtOH \text{ or } C_2H_6 \quad (12)$$

the proposed reaction mechanisms is considered to be the major film-forming precursor but due to its strong reactivity is very unstable[71−73] and therefore undetectable by GC/MS. The hydrogen abstraction reactions postulated by eqs 10 and 11 are consistent with the chemiluminescence spectra of the gas phase recorded in the reactor during ROP−CVD. A typical chemiluminescence spectrum, exemplified in Figure 8, reveals the presence of a very intense peak at 306 nm and a lower intensity peak at 281 nm attributed to the $OH(A^2\Sigma^+) \rightarrow OH(X^2\Pi)$ transition,[74] thus pointing to a high concentration of hydroxyl radicals in the gas phase. It is worth

(71) Raabe, G.; Michl, J. *Chem. Rev.* **1985**, *85*, 419.
(72) Raabe, G.; Michl, J. In *The Chemistry of Organic Silicon Compounds*; Patai, S., Rappoport, Z., Eds.; Wiley: New York, 1989; Chapter 17.
(73) Apeloig, Y. In *The Chemistry of Organic Silicon Compounds*; Patai, S., Rappoport, Z., Eds.; Wiley: New York, 1989; Chapter 2.
(74) Pearse, R. W. B.; Gaydon, A. G. *The Identification of Molecular Spectra*; Chapman & Hall: London, 1976; p 264.

mentioning that the conversion of TEOS to diethoxy-silanone via similar reaction mechanisms to those described by eqs 10 and 12 has been proposed by Desu[75] for thermal CVD.

An attack by the excited oxygen atom $O(^1D)$ on the primary carbon atom in the TEOS, involving the elimination of molecular hydrogen and the formation of an aldehyde group,[67] may also take place (eq 13).

$$O(^1D) + (EtO)_4Si \longrightarrow \left[(EtO)_3SiOCH_2\text{-}HC \overset{H\cdots H}{\cdots} O \right]^{\ddagger}$$

$$\longrightarrow (EtO)_3SiOCH_2CHO + H_2 \qquad (13)$$

Equation 13 is consistent with the presence of 2-(tri-ethoxysilyloxy)acetaldehyde, the abundant low-molec-ular-weight product of TEOS conversion (compound 7, Table 6).
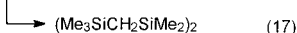
3.5. Oligomerization Step. Owing to equivalent biradical and biionic structures ascribed to the silene ($>Si{=}C< \leftrightarrow >\!^\bullet Si{-}C^\bullet< \leftrightarrow >\!^+Si{-}C^-<$)[71−73] and silanone ($>Si{=}O \leftrightarrow >\!^\bullet Si{-}O^\bullet \leftrightarrow >\!^+Si{-}O^-$)[71−73] units, 1,1-dimeth-ylsilene and diethoxysilanone precursors formed via conversion of the respective source compounds have the nature of the classic bifunctional monomers and, there-fore, they can easily undergo the gas-phase oligomer-ization in the investigated remote plasma CVD pro-cesses.

RHP−CVD. The oligomerization of 1,1-dimethylsilene reasonably explains the formation of some low-molec-ular-weight and oligomeric products identified by GC/MS. The presence of 1,1,3,3-tetramethyl-1,3-disilacy-clobutane $(Me_2SiCH_2)_2$ among the conversion products of HMDS (compound 5, Table 4) and TrMS (compound 3, Table 5) is indicative of a "head-to-tail" dimerization of 1,1-dimethylsilene.[71−73,76] The dimerization (eq 14) is

$$2Me_2Si{=}CH_2 \longrightarrow Me_2Si\diamondsuit SiMe_2 \qquad (14)$$
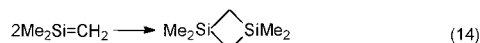
a strongly exothermic reaction ($\Delta H = -318$ kJ mol^{-1} and energy barrier $E_a = 36$ kJ mol^{-1} for $H_2Si{=}CH_2$).[73]

A stepwise insertion of 1,1-dimethylsilene precursor into either a nonpolar Si−Si bond or a slightly polar Si−C bond, respectively, in HMDS and the resulting product may take place[71−73] (eqs 15−17). Equation 15

$$Me_2SiCH_2 + Me_3SiSiMe_3 \rightarrow Me_3SiSiMe_2CH_2SiMe_3 \qquad (15)$$

$$Me_2SiCH_2 + Me_3SiSiMe_2CH_2SiMe_3 \longrightarrow Me_3Si(Me_2SiCH_2)_2SiMe_3 \qquad (16)$$
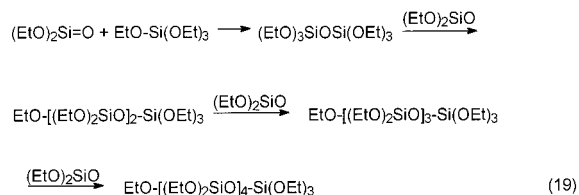
$$\longrightarrow (Me_3SiCH_2SiMe_2)_2 \qquad (17)$$

explains the formation of the compound numbered by 10 or 14 in Tables 4 and 5, respectively, whereas eqs 16 and 17 account for the formation of compounds 12 and 13, respectively, in Table 4.

An insertion of 1,1-dimethylsilene precursor into the Si−H bond in TrMS (eq 18) reasonably explains the formation of compound numbered by 4 or 2 in Tables 3 and 4, respectively.

$$Me_2SiCH_2 + HSiMe_3 \rightarrow Me_2HSiCH_2SiMe_3 \qquad (18)$$

ROP−CVD. Diethoxysilanone precursor may easily undergo oligomerization reaction with TEOS by a "head-to-tail" insertion of silanone unit to the Si−O bond[71−73,77] and further stepwise heterooligomerization, thus propa-gating the diethoxysiloxane chain (eq 19). The oligo-

$$(EtO)_2Si{=}O + EtO\text{-}Si(OEt)_3 \longrightarrow (EtO)_3SiOSi(OEt)_3 \xrightarrow{(EtO)_2SiO}$$

$$EtO\text{-}[(EtO)_2SiO]_2\text{-}Si(OEt)_3 \xrightarrow{(EtO)_2SiO} EtO\text{-}[(EtO)_2SiO]_3\text{-}Si(OEt)_3$$

$$\xrightarrow{(EtO)_2SiO} EtO\text{-}[(EtO)_2SiO]_4\text{-}Si(OEt)_3 \qquad (19)$$

merization described by eq 19 explains well the forma-tion of identified linear siloxane oligomers 12, 15, 17, and 18 (Table 6). It is noteworthy that dimer 12 and trimer 15 have also been detected by GC/MS in the gas phase of the TEOS thermal CVD process.[78]

Another reaction of diethoxysilanone that may rapidly occur is a "head-to-tail" dimerization, a strongly exo-thermic process ($\Delta H = -458$ kJ mol^{-1} in the case of H_2-Si$=$O) proceeding with no energetic barrier[73] (eq 20).

$$2(EtO)_2Si{=}O \rightleftharpoons (EtO)_2Si\overset{O}{\underset{O}{<}}Si(EtO)_2 \qquad (20)$$
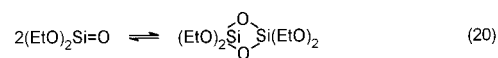
However, the cyclic dimer resulting from eq 20, due to a highly strained four-membered siloxane ring,[79] is a reactive, transient intermediate that may readily un-dergo stepwise ring-expansion reaction, via an insertion mechanism involving diethoxysilanone[71−73,77] (eq 21).

$$[(EtO)_2SiO]_2 \xrightarrow{(EtO)_2SiO} [(EtO)_2SiO]_3 \xrightarrow{(EtO)_2SiO} [(EtO)_2SiO] \qquad (21)$$
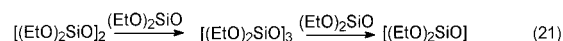
The oligomerization described by eq 21 is consistent with the presence of cyclic trimer 14 and tetramer 16 (Table 6). As can be inferred from the data in Table 6, the total concentration of linear oligomers (12, 13, 15, 17, and 18) is higher than that of the cyclic compounds (14 and 16) by nearly 1 order of magnitude. This observation suggests that the siloxane chain propaga-tion (eq 19) prevails over the cyclization (eq 20) and ring-expansion (eq 21) reactions in the oligomerization step.

A competitive hydrolysis−polycondensation mecha-nism for the formation of identified linear and cyclic siloxane oligomers seems to be of lesser importance for the investigated ROP−CVD. According to the chemistry of polysiloxanes,[80] the hydrolysis of Si−O bonds and the subsequent polycondensation process requires the con-tribution of either nucleophilic or electrophilic agents. The study of the gas-phase hydrolysis and polyconden-sation of TEOS in the presence of acidic or basic

(75) Desu, S. B. *J. Am. Ceram. Soc.* **1989**, *72*, 1615.

(76) Fritz, G.; Matern, E. *Carbosilanes*; Springer-Verlag: Berlin, 1986; Chapter 2.

(77) Voronkov, M. G.; Basenko, S. V. *J. Organomet. Chem.* **1995**, *500*, 325.

(78) Satake, T.; Sorita, T.; Fujioka, H.; Adachi, H.; Nakajima, H. *Jpn. J. Appl. Phys.* **1994**, *33*, 3339.

(79) Grabbe, A.; Michalske, T. A.; Smith, W. L. *J. Phys. Chem.* **1995**, *99*, 4648.

(80) Chojnowski, J. In *Siloxane Polymers*; Clarson, S. J., Semlyen, J. A., Eds.; PTR Prentice Hall: Englewood Cliffs, NJ, 1993; Chapter 1.
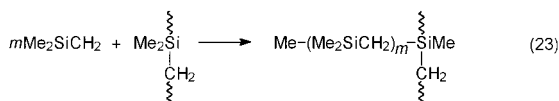
catalysts indeed revealed that the process is ineffective when the catalysts are absent.[81,82]

3.6. Hypothetical Polymerization Step. In light of the oligomerization reactions discussed above, we assume that 1,1-dimethylsilene and diethoxysilanone precursors contribute to the growth of the a-Si:C:H and a-SiO$_2$ films, respectively, via surface polymerization predominantly involving a polyinsertion mechanism.

RHP–CVD. A hypothetical growth of the a-Si:C:H film may take place via a stepwise insertion of 1,1-dimethylsilene precursor (formed from HMDS and TrMS in the initiation step) to the Si–Si, Si–H, and Si–C bonds in the source compound or oligomer molecules adsorbed on the growth surface. This process propagates linear carbosilane segments $-(Me_2SiCH_2)_n-$ in the deposit and may be exemplified by eq 22, which describes schematically a "head-to-tail" polyinsertion of 1,1-dimethylsilene to the methylsilyl group. Branching
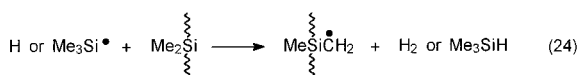
$$n Me_2SiCH_2 \; + \; Me{-}\overset{|}{\underset{|}{Si}}{-} \; \longrightarrow \; Me{-}(Me_2SiCH_2)_n{-}\overset{|}{\underset{|}{Si}}{-} \tag{22}$$
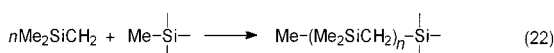
the linear carbosilane segments via an analogous polyinsertion reaction may also take place (eq 23). Reactions

$$m Me_2SiCH_2 \; + \; Me_2\overset{\wr}{\underset{\overset{|}{CH_2}}{Si}} \; \longrightarrow \; Me{-}(Me_2SiCH_2)_m{-}\overset{\wr}{\underset{\overset{|}{CH_2}}{SiMe}} \tag{23}$$

described by eqs 22 and 23 predominate at low substrate temperature and are consistent with the presence in the FTIR spectra of the a-Si:C:H films (Figure 4) of a very strong absorption band with maximum in the range 1030–1020 cm^{-1}, which mostly originates from the Si–CH$_2$–Si units.
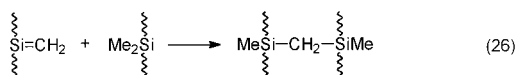
Reaction between atomic hydrogen or trimethylsilyl radicals (formed via eqs 3, 4, 9) and methylsilyl groups in carbosilane segments may result in the abstraction of hydrogen (eq 24). The radical structure formed in eq

$$H \; or \; Me_3Si^{\bullet} \; + \; Me_2\overset{\wr}{\underset{\wr}{Si}} \; \longrightarrow \; Me\overset{\bullet}{Si}CH_2 \; + \; H_2 \; or \; Me_3SiH \tag{24}$$

24 may readily be converted into a silene unit via an endothermic reaction[71,72,76] involving the elimination of a methyl group (eq 25). The methyl radicals effusing

$$Me\overset{\wr}{\underset{\wr}{\overset{\bullet}{Si}}}CH_2 \; \longrightarrow \; \overset{\wr}{\underset{\wr}{Si}}{=}CH_2 \; + \; Me^{\bullet} \tag{25}$$
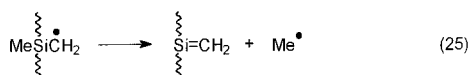
from the film may react with methylsilyl groups to produce an intermediate radical structure as in eq 24. The reaction described by eq 25 is particularly important because it involves the elimination of organic moieties from the film. The solid-state phase reactions of the silene units with the Si–Me groups in the vicinal carbosilane segments of the film (via an insertion mechanism) spontaneously contribute to the first step of cross-linking (eq 26). According to the thermodynamic

$$\overset{\wr}{\underset{\wr}{Si}}{=}CH_2 \; + \; Me_2\overset{\wr}{\underset{\wr}{Si}} \; \longrightarrow \; Me\overset{\wr}{\underset{\wr}{Si}}{-}CH_2{-}\overset{\wr}{\underset{\wr}{Si}}Me \tag{26}$$

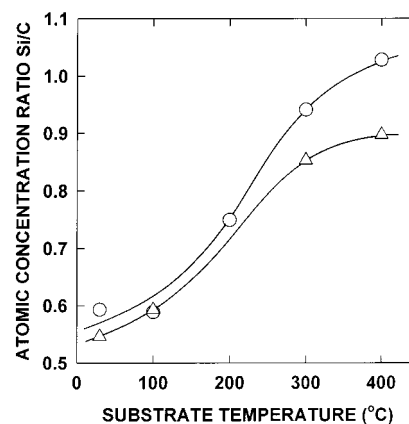data[60] the polymerization (eqs 22 and 24) and cross-

Figure 9. AES atomic concentration ratio Si/C determined for the bulk of the film deposited from HMDS (○) and TrMS (△) as a function of the substrate temperature.
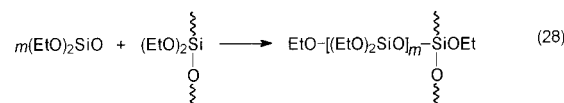
linking (eq 26) reactions contributing to the a-Si:C:H film growth are assumed to be exothermic.

The dehydrogenation of the carbosilane cross-links at high deposition temperature regime, resulting in the formation of carbosilane units with tertiary and quaternary carbon atoms (Si$_3$CH and Si$_4$C, respectively), leads to the formation of a three-dimensional Si-carbidic network structure. This is confirmed by the evolution of the a-Si:C:H film structure taking place with increasing T_S, as revealed by our earlier FTIR[21] and present AES observations: (*i*) A marked increase in the intensity of the IR band in 830–800 cm^{-1}, arising from the Si–C carbidic bonds, accompanied by a drastic drop in the intensity of the band in 2960–2900 cm^{-1}, attributed to the C–H bonds.[21] (*ii*) An increase of the AES atomic concentration ratio Si/C to the value close to that of stoichiometric silicon carbide (Figure 9).
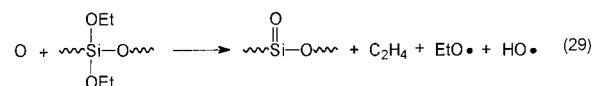
ROP–CVD. A hypothetical mechanism for silica film growth seems to be involved in the surface reaction of diethoxysilanone precursor with ethoxysilyl groups in TEOS and oligomeric molecules adsorbed on the growth surface. This process described schematically by eq 27 leads

$$n(EtO)_2SiO \; + \; EtO{-}\overset{|}{\underset{|}{Si}}{-} \; \longrightarrow \; EtO{-}[(EtO)_2SiO]_n{-}\overset{|}{\underset{|}{Si}}{-} \tag{27}$$
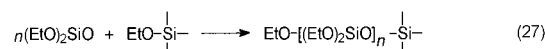
to the propagation of polydiethoxysiloxane segments via an insertion mechanism. Branching the linear segments via analogous polyinsertion reaction may also take place (eq 28). The ethoxysilyl groups in the siloxane segments

$$m(EtO)_2SiO \; + \; (EtO)_2\overset{\wr}{\underset{\overset{|}{O}}{Si}} \; \longrightarrow \; EtO{-}[(EtO)_2SiO]_m{-}\overset{\wr}{\underset{\overset{|}{O}}{Si}}OEt \tag{28}$$

may undergo conversion to silanone units via the reaction with the atomic oxygen (eq 29). This process is

$$O \; + \; \text{\small\raisebox{0ex}{$\sim$}}\overset{OEt}{\underset{OEt}{Si}}{-}O\text{\small\raisebox{0ex}{$\sim$}} \; \longrightarrow \; \text{\small\raisebox{0ex}{$\sim$}}\overset{\overset{O}{\parallel}}{Si}{-}O\text{\small\raisebox{0ex}{$\sim$}} \; + \; C_2H_4 \; + \; EtO^{\bullet} \; + \; HO^{\bullet} \tag{29}$$

of particular importance because it eliminates the

(81) Campostrini, R.; Carturan, G.; Pelli, B.; Traldi, P. *J. Non-Cryst. Solids* **1989**, *108*, 143.

(82) Campostrini, R.; Carturan, G.; Soraru, G.; Traldi, P. *J. Non-Cryst. Solids* **1989**, *108*, 315.
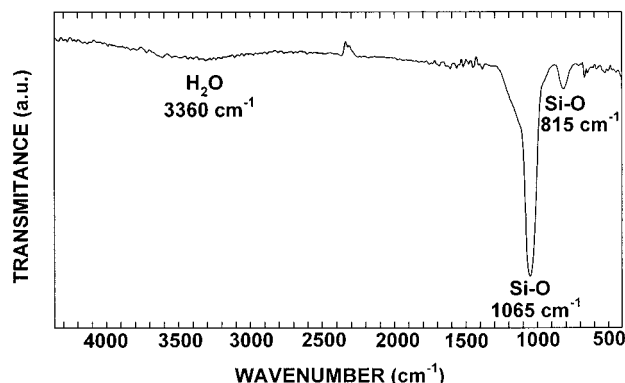
Figure 10. FTIR spectrum of a 480-nm-thick a-SiO$_2$ film deposited from TEOS on a c-Si at T_S = 300 °C.

organic moieties from the film and appears to be consistent with a structural study by Hatanaka et al.,[83] which has shown very low organic content in the film deposited from TEOS, even onto an unheated substrate. Moreover, the insertion of silanone units (formed as in eq 29) into the Si−OEt bonds in the vicinal polysiloxane segments contribute to the cross-linking process. The elementary cross-linking reaction between the structure segments is presented in eq 30. On the basis of the

$$\text{Si=O} \ + \ \text{EtO–Si–OEt} \longrightarrow \text{EtOSi–O–SiOEt} \qquad (30)$$
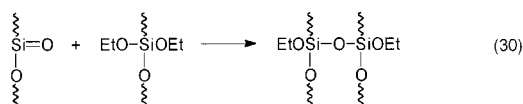
thermodynamic data,[60] the polyinsertion (eqs 27 and 28) and cross-linking (eq 30) processes taking place in the silica film growth are considered to be exothermic.

The proposed primary steps of silica film growth are strongly affected by the substrate temperature. The increase of T_S promotes the heterogeneous (gas−solid) and homogeneous (solid−solid) reactions (exemplified by eqs 27−30, respectively), leading to a silica network structure in the film. This is supported by the structural data in Figure 10 , which presents a typical FTIR spectrum of a silica film deposited from TEOS at T_S = 300 °C. The spectrum exhibits a strong absorption band at 1065 cm^{-1}, with a half-width of 88 cm^{-1}, and a distinct band at 815 cm^{-1}, both characteristic of the Si−O bonds in silicon dioxide.[84] A broad band with a maximum at 3360 cm^{-1} is attributed to water absorbed in the film.[84] Bands that might originate from the C−H, Si−H, and Si−C bonds are not detected. The FTIR data point to the formation of a silica network structure in the film.

4. Conclusions

The presented results account for a substantial role of the polymerization reactions in the formation of the a-Si:C:H and a-SiO$_2$ thin-film materials from organosilicon sources in the RHP−CVD and ROP−CVD processes, respectively. The source compound is converted to a transient "hot" intermediate with the nature of a bifunctional monomer, which may readily undergo polymerization.

In the case of RHP−CVD, the precursor formation step proceeds via cleavage of the Si−Si and Si−H bonds in the HMDS and TrMS molecules, respectively. The rate constant values of the RHP−CVDs evaluated for HMDS and TrMS reveal an extremely high reactivity of the Si−H bond in an atomic hydrogen environment and account for TrMS as a very effective source compound for the production of a-Si:C:H films. The oligomeric structures identified by GC/MS and the chemistry of the oligomerization step imply the gas-phase conversion of HMDS and TrMS to 1,1-dimethylsilene, Me$_2$Si=CH$_2$, as the a-Si:C:H film-forming precursor. Because of a high-reactivity π-bond in the silene unit, the precursor may easily undergo surface polymerization via an insertion mechanism, propagating carbosilane, −(Me$_2$SiCH$_2$)$_n$−, segments in the deposit. The silene units may also be formed in the deposit by the reaction of the gas-phase radicals with methylsilyl groups in the growing carbosilane segments. The solid-state phase insertion of the >Si=CH$_2$ units to the Si−Me bonds in the vicinal carbosilane segments contributes to the spontaneous cross-linking via carbosilane Si−CH$_2$−Si cross-links. The dehydrogenation of the cross-links in a high deposition temperature regime leads to the formation of a Si−carbidic network structure.

In the case of ROP−CVD, the growth rate of silica film is proportional to the concentration of atomic oxygen. No observed effect of the type of atomic oxygen on the growth rate of silica film suggests that both atomic oxygen components, ground-state O(^{3}P) and excited-state O(^{1}D), contribute to the precursor formation step via the same mechanism. The abstraction of the hydrogen atom from the TEOS molecule is a major reaction to the precursor formation. The oligomeric products identified by GC/MS and the chemistry involved in their formation provide strong evidence for the gas-phase conversion of TEOS to diethoxysilanone (EtO)$_2$Si=O, high-reactivity precursor of silica film growth. Surface polymerization of the adsorbed diethoxysilanone precursor via an insertion mechanism, resulting in the formation of polydiethoxysiloxane −[(EtO)$_2$SiO]$_n$−segments, is assumed to be the primary step of silica film growth. Conversion of ethoxysilyl units in the growing film to silanone groups, strongly cross-linking agents, seems to be a driving force of silica network formation.

CM001044+

(83) Wickramanayaka, S.; Matsumoto, A.; Nakanishi, Y.; Hosokawa, N.; Hatanaka, Y. *Jpn. J. Appl. Phys.* **1994**, *33*, 3520.
(84) Pliskin, W. A. *J. Vac. Sci. Technol.* **1977**, *14*, 1064.